Black hole scaling relations of active and quiescent galaxies: Addressing selection effects and constraining virial factors

Francesco Shankar,[1]★ Mariangela Bernardi,[2] Kayleigh Richardson,[1]
Christopher Marsden,[1] Ravi K. Sheth,[2] Viola Allevato,[3] Luca Graziani [ID],[4]
Mar Mezcua [ID],[5,6] Federica Ricci [ID],[7] Samantha J. Penny [ID],[8] Fabio La Franca[9] and
Fabio Pacucci [ID][10]

[1]*Department of Physics and Astronomy, University of Southampton, Highfield SO17 1BJ, UK*
[2]*Department of Physics and Astronomy, University of Pennsylvania, 209 South 33rd St, Philadelphia, PA 19104, USA*
[3]*Scuola Normale Superiore, Piazza dei Cavalieri 7, I-56126 Pisa, Italy*
[4]*Dipartimento di Fisica, Sapienza Università di Roma, Piazzale Aldo Moro 5, I-00185 Roma, Italy*
[5]*Institute of Space Sciences (ICE, CSIC), Campus UAB, Carrer de Magrans, E-08193 Barcelona, Spain*
[6]*Institut d'Estudis Espacials de Catalunya (IEEC), Carrer Gran Capità, E-08034 Barcelona, Spain*
[7]*Instituto de Astrofísica and Centro de Astroingeniería, Facultad de Física, Pontificia Universidad Católica de Chile, Casilla 306, Santiago 22, Chile*
[8]*Institute of Cosmology and Gravitation, University of Portsmouth, Dennis Sciama Building, Burnaby Road, Portsmouth PO1 3FX, UK*
[9]*Dipartimento di Matematica e Fisica, Università Roma Tre, via della Vasca Navale 84, I-00146 Roma, Italy*
[10]*Department of Physics, Yale University, New Haven, CT 06511, USA*

ABSTRACT

Local samples of quiescent galaxies with dynamically measured black hole masses (M_{bh}) may suffer from an angular resolution-related selection effect, which could bias the observed scaling relations between M_{bh} and host galaxy properties away from the intrinsic relations. In particular, previous work has shown that the observed M_{bh}–M_{star} relation is more strongly biased than the M_{bh}–σ relation. Local samples of active galactic nuclei (AGN) do not suffer from this selection effect, as in these samples M_{bh} is estimated from megamasers and/or reverberation mapping-based techniques. With the exception of megamasers, M_{bh} estimates in these AGN samples are proportional to a virial coefficient f_{vir}. Direct modelling of the broad-line region suggests that $f_{vir} \sim 3.5$. However, this results in an M_{bh}–M_{star} relation for AGN, which lies below and is steeper than the one observed for quiescent black hole samples. A similar though milder trend is seen for the M_{bh}–σ relation. Matching the high-mass end of the M_{bh}–M_{star} and M_{bh}–σ relations observed in quiescent samples requires $f_{vir} \gtrsim 15$ and $f_{vir} \gtrsim 7$, respectively. On the other hand, $f_{vir} \sim 3.5$ yields M_{bh}–σ and M_{bh}–M_{star} relations for AGN, which are remarkably consistent with the expected 'intrinsic' correlations for quiescent samples (i.e. once account has been made of the angular resolution-related selection effect), providing additional evidence that the sample of local quiescent black holes is biased. We also show that, as is the case for quiescent black holes, the M_{bh}–M_{star} scaling relation of AGN is driven by σ, thus providing additional key constraints to black hole–galaxy co-evolution models.

Key words: black hole physics – galaxies: fundamental parameters – galaxies: nuclei – galaxies: structure.

1 INTRODUCTION

It has long been accepted that active galactic nuclei (AGN), the central powerhouses of the most energetic galaxies in the Universe, are powered by the release of gravitational energy during the accretion of material on to the supermassive black hole at their centres. The general consensus is that most, if not all, galaxies host a massive black hole and may go through an AGN 'phase'. The latter may be self-regulating both the black hole growth and star formation in the host galaxy via some wind/jet-driven feedback mechanisms

★ E-mail: F.Shankar@soton.ac.uk

(see reviews by, e.g. Shankar 2009 and Alexander & Hickox 2012). Models predict that an AGN and its host may coevolve (e.g. Silk & Rees 1998; Granato et al. 2004), leading to host characteristics such as galaxy bulge/total stellar mass (M_{bulge}/M_{star}) and/or central stellar velocity dispersion (σ) being linked to black hole mass (M_{bh}). Probing these relations is a primary goal of modern cosmology because its understanding will be a crucial step towards a more complete view of galaxy evolution.

Many groups have quantified scaling relations between super-massive black hole masses and host galaxy properties, in the local Universe, using samples of *quiescent* galaxies (see e.g. Ferrarese & Ford 2005; Kormendy & Ho 2013; Graham 2016). However, Bernardi et al. (2007) showed that the $\sigma-M_{star}$ relations defined by quiescent black hole samples differ from that defined by the bulk of the galaxies in the Sloan Digital Sky Survey (SDSS; York et al. 2000). van den Bosch et al. (2015) and Shankar et al. (2016) confirmed that quiescent samples are biased towards dense galaxies. As a result, it has been suggested that measurements of the M_{bh} scaling relations in these samples may be severely biased (e.g. Bernardi et al. 2007; Gültekin et al. 2009; Batcheldor 2010; Morabito & Dai 2012; Shankar et al. 2016).

In these galaxies, M_{bh} is estimated from the dynamics of stars near the black hole 'sphere of influence' (e.g. Merritt & Ferrarese 2001a):

$$r_{infl} \equiv GM_{bh}/\sigma^2 . \tag{1}$$

Since r_{infl} is small (order of parsecs), insufficient resolution prevents reliable black hole mass estimates or forces to target only the largest black holes, possibly leading to a selection bias. Shankar et al. (2016) used Monte Carlo simulations to show that this resolution-related selection effect has the potential to artificially increase the normalization of the $\sigma-M_{star}$ and $M_{bh}-\sigma$ relation by a factor of a few, and the $M_{bh}-M_{star}$ by an order of magnitude or more. Indeed, this selection effect alone can go a long way towards explaining why, to date, pulsar timing arrays have failed to detect any gravitational waves from supermassive black hole mergers (Sesana et al. 2016).

To gather more robust constraints on black hole–galaxy coevolution models, it is thus necessary to analyse samples that do not suffer from this resolution-related selection effect. In active galaxies, M_{bh} can be estimated spectroscopically from the kinematics of the broad-line region (BLR) or gas orbiting around the very inner regions around the central black hole (e.g. Ferrarese & Ford 2005). However, except for masers for which black hole masses can be inferred from rotation curves (e.g. Ferrarese & Ford 2005), for the vast majority of (Type 1) AGN, black hole masses are derived from the (presumed) virial motions of the BLR gas cloud orbiting in the vicinity of the central compact object:

$$M_{bh} = f_{vir} \frac{r\,(\Delta V)^2}{G}. \tag{2}$$

In equation (2), r is the radius of the BLR, which is derived from reverberation mapping (e.g. Blandford & McKee 1982; Peterson 1993), or reverberation-based methods that use the radius–luminosity relation (e.g. Bentz et al. 2006). The characteristic velocity ΔV is derived from the width of the emission lines (a common one is Hβ), and G is the gravitational constant. As motions in the BLR are not perfectly Keplerian, a parameter f_{vir} is included in equation (2) to account for the uncertainties in kinematics, geometry, and inclination of the clouds (e.g. Ho & Kim 2014, and references therein). Systematically different values of f_{vir} can be found if the virial masses (based on reverberation mapping campaigns) are computed using the full width at half-maximum

(FWHM) or dispersion of the emission line (e.g. Onken et al. 2004; Collin et al. 2006). In what follows, we will always refer to f_{vir} as the virial factor calibrated on the line dispersion (i.e. second moment of the line profile) of Hβ (e.g. Peterson et al. 2004).

A reasonable guess for f_{vir} is obtained by matching the AGN black hole scaling relations to those of inactive black holes. Typical values for line dispersion-based f_{vir} derived from the match to the $M_{bh}-\sigma$ relation of quiescent black holes are in the range $f_{vir} \sim 4$–5 (e.g. Onken et al. 2004; Woo et al. 2010a; Grier et al. 2013; Batiste et al. 2017, and references therein). Although lower values for f_{vir} have also been claimed (Graham et al. 2011), Ho & Kim (2014) invoke larger values, $f_{vir} \sim 6$–10, when comparing AGN in classical bulges to the quiescent sample of Kormendy & Ho (2013). In cases in which the BLR structure and dynamics have been modelled directly, the virial coefficient can be constrained directly from the data. Following the geometric and dynamic modelling put forward by Pancoast, Brewer & Treu (2014), Grier et al. (2017) have fitted the line dispersion of the Hβ emission-line spectra of four sources finding a mean $f_{vir} \sim 3.5$ ($\log f_{vir} = 0.54 \pm 0.17$). Williams et al. (2018) have more recently confirmed an average value of $f_{vir} \sim 3.7$ ($\log f_{vir} = 0.57 \pm 0.19$) when fitting the H$\beta$ line dispersion of another seven AGN. The latter values are systematically lower than those found by, e.g. Ho & Kim (2014). Clearly, to date, there is no consensus on the best value of f_{vir} for weighing black holes in AGN.

To use AGN as reliable probes of black hole–galaxy scaling relations, more secure determinations of f_{vir} are required. The main aim of this work is to take a step in this direction. To this end, we analyse scaling relations in a variety of local AGN samples, so as to probe their level of bias with respect to a larger sample of local galaxies from the SDSS. We briefly describe how we homogenize the samples in Section 2, and provide full details in Appendix A. Section 3 presents scaling relations of the properties of the galaxies that host AGN – to address the question of whether these are a biased subset – before considering scaling relations with M_{bh} and their implications for f_{vir}. It should be noted in fact that since resolution-related selection effects have a stronger impact on the quiescent $M_{bh}-M_{star}$ relation rather than on the $M_{bh}-\sigma$ one (Shankar et al. 2016), if such selection effects are present, systematically different mean values of f_{vir} should be derived when calibrating AGN samples against the $M_{bh}-\sigma$ or the $M_{bh}-M_{star}$ relations of local inactive black hole samples. In this work, we show that such a systematic offset in f_{vir} is indeed present, but the offset can be removed by accounting for the resolution-related selection effect.

Throughout, we adopt $h = 0.7$, $\Omega_m = 0.3$, and $\Omega_\Lambda = 0.7$ for the SDSS sample. All AGN samples considered here have black holes and host galaxy properties derived assuming identical or very similar cosmological parameters.[1]

2 HOMOGENIZING DIFFERENT DATA SETS

In this work, we consider a number of serendipitous local AGN samples. These were collected at different flux limits and with different host galaxy morphologies. Therefore, it is important to homogenize them so that their M_{star} and M_{bh} values can be meaningfully compared. We clarify that throughout this paper M_{star} always refers to the *total* stellar mass of a galaxy, while M_{bulge} refers to its bulge stellar mass.

---

[1]The largest offset is found for the Ho & Kim (2014) sample that adopts $h = 0.705$ and $\Omega_m = 0.27$ for calibrating distances, which anyway induce only ~ 0.5 per cent difference in distances at the redshifts of interest here.

Table 1. List of the data sets used throughout this paper.

Data acronym	Method	Reference
	Active	
H&K	Reverberation	Ho & Kim (2014)
MN&M	Single epoch	Martín-Navarro & Mezcua (2018)
VdB	Single epoch	van den Bosch (2016)
VdB	Masers	van den Bosch (2016)
G +	Masers	Greene et al. (2016)
B +	Single epoch	Busch et al. (2014)
R&V	Single epoch	Reines & Volonteri (2015)
B&MN	Single epoch	Bentz & Manne-Nicholas (2018)
	Quiescent	
Sa +	Dynamical	Savorgnan & Graham (2016)
K&	Dynamical	Kormendy & Ho (2013)

For our study, we correct all total stellar mass estimates so they correspond to M_{star}/L from Bell et al. (2003a) and a Chabrier initial mass function (IMF; Chabrier 2003) since this was the choice made by Shankar et al. (2016) in their study of the *intrinsic* (i.e. unbiased) black hole scaling relations. We use velocity dispersions[2] $\sigma = \sigma_e = \sigma(R_e)$ measured within the galaxy optical effective radius R_e. For the quiescent and some active black hole samples, we correct velocity dispersions measured within an aperture of radius R to the value they are expected to have within an aperture of one effective radius using the Sérsic index-dependent correction $\sigma(R_e) \propto (R/R_e)^{\gamma(n_{Ser})}$ (Bernardi et al. 2017b). Finally, if not otherwise specified (as for the sample from Martín-Navarro & Mezcua 2018), wherever relevant we assume $f_{vir} = 3.5$, following the Lick monitoring project (Walsh et al. 2009) and the latest results of Grier et al. (2017) and Williams et al. (2018) when adopting the H β line dispersion. The Appendix provides details of these corrections for the different samples we use. A list of the data sets considered in this work is given in Table 1.

3 RESULTS

3.1 The $\sigma - M_{star}$ relation of active galaxies

The first step of our analysis is to compare the $\sigma - M_{star}$ relation of the different AGN samples among themselves and with that of a much larger sample of galaxies from the SDSS. The purpose of this check is twofold. First, we ensure that at least for the AGN samples with available (total) stellar mass and velocity dispersion measurements, the homogenizing corrections mentioned in Section 2, and expanded in Appendix A, provide consistent results. Secondly, we probe by how much, if at all, active host galaxies differ in terms of stellar mass and/or velocity dispersion from the general population of SDSS galaxies. In fact, as mentioned in Section 1, Bernardi et al. (2007) and Shankar et al. (2016) showed that local inactive galaxies with dynamical black hole mass measurements (the open black and red squares and the brown triangles in Fig. 1) tend to have, on average, larger velocity dispersions compared to counterpart galaxies in the SDSS. This behaviour can be in large part explained by the selection effect imposed by limited telescope resolution power, which forces to preferentially target more massive black holes, predominantly hosted in galaxies with larger velocity dispersions (Shankar et al. 2016; Barausse et al. 2017; Shankar, Bernardi & Sheth 2017)

Fig. 1 shows[3] that reassuringly, after applying the proper homogenizing corrections in stellar mass and velocity dispersion, almost all the classical and pseudobulges from Ho & Kim (2014; the filled red circles and the green squares, respectively), the megamasers from Greene et al. (2016; the filled cyan stars), and the active galaxies in the van den Bosch (2016; the blue diamonds and the cyan circles for reverberation-based and masers AGN, respectively) sample, fall within the scatter (see also Grier et al. 2013, their fig. 4, for a similar result) of the SDSS velocity dispersion–stellar mass relation (magenta long-dashed and dotted lines). For the SDSS galaxies, we adopt the latest rendition of the Meert, Vikram & Bernardi (2015) galaxy sample, with light profiles extracted from Sérsic + exponential models and mass-to-light ratios from Mendel et al. (2013). We increase all stellar masses by an average 0.05 dex (see fig. A2 in Bernardi et al. 2017a) to account for the (small) difference at high stellar masses with the Bell et al. (2003b) mass-to-light ratios used by Shankar et al. (2016) and adopted as a reference in this work. Some of the lower mass pseudobulges from Ho & Kim (2014; the green squares) and all the low-mass Seyferts from Martín-Navarro & Mezcua (2018; the orchid upside down triangles) tend to have, on average, somewhat lower velocity dispersions at fixed stellar mass by $\lesssim 0.05 - 0.1$ dex, better lining up, as expected, with the SDSS $\sigma - M_{star}$ relation of late-type galaxies (the brown dashed line). The latter was calibrated out of the subsample of SDSS galaxies with a high probability $P(\text{Scd}) > 0.7$ of being classified as late spirals according to the Bayesian automated classification of Huertas-Company et al. (2011).

In the right-hand panel of Fig. 1, we also include the black hole sample[4] of elliptical galaxies from Kormendy & Ho (2013; the red open squares). First off, it is relevant to note that the Kormendy & Ho (2013) ellipticals broadly overlap with the early types from the Savorgnan & Graham (2016; the open black squares) black hole sample and lie substantially above the mean $\sigma - M_{star}$ relation of SDSS galaxies. Shankar et al. (2016) also showed that other samples of black holes in inactive galaxies (Beifiori et al. 2012; McConnell & Ma 2013; Läsker et al. 2014) lie systematically above the SDSS $\sigma - M_{star}$ relation, further supporting the view that such a mismatch is not a result of different choices in stellar mass calibrations and/or apertures, but an underlying selection effect affecting the sample of black holes in local inactive galaxies with dynamical mass measurement. It is particularly meaningful to compare the Kormendy & Ho (2013) ellipticals with the van den Bosch (2016) sample. Both samples adopt exactly the same mass-to-light ratio and span a similar range in stellar mass $10 \lesssim \log M_{star}/M_\odot \lesssim 11.5$, yet the Kormendy & Ho (2013) data points are placed at significantly larger velocity dispersions. Whilst some of the offset between the two samples can be ascribed to simple morphological segregation, being the van den Bosch (2016) AGN sample dominated by Seyfert-like galaxies that tend to be characterized by lower velocity dispersions (see left-hand panel),

---

[2]Unless otherwise noted, throughout this work σ always refers to the velocity dispersion within one effective radius R_e, $\sigma_e \equiv \sigma(R_e)$.

[3]For simplicity, in this and in all subsequent figures, to distinguish them from masers (labelled as 'mas'), we label as 'rev' all AGN samples in which black hole masses are based on direct reverberation mapping or reverberation-based (i.e. single-epoch virial) techniques.

[4]We slightly correct the stellar masses in the Kormendy & Ho (2013) sample to match the K-band mass-to-light ratios to convert from dynamical to stellar masses and the same IMF (see text after equation A4). Velocity dispersions are also corrected from $0.5R_e$ to R_e following Cappellari et al. (2006). We note that such corrections are relatively small and, if neglected, would further exacerbate the tension between the Kormendy & Ho (2013) sample and the SDSS and van den Bosch (2016) galaxies.
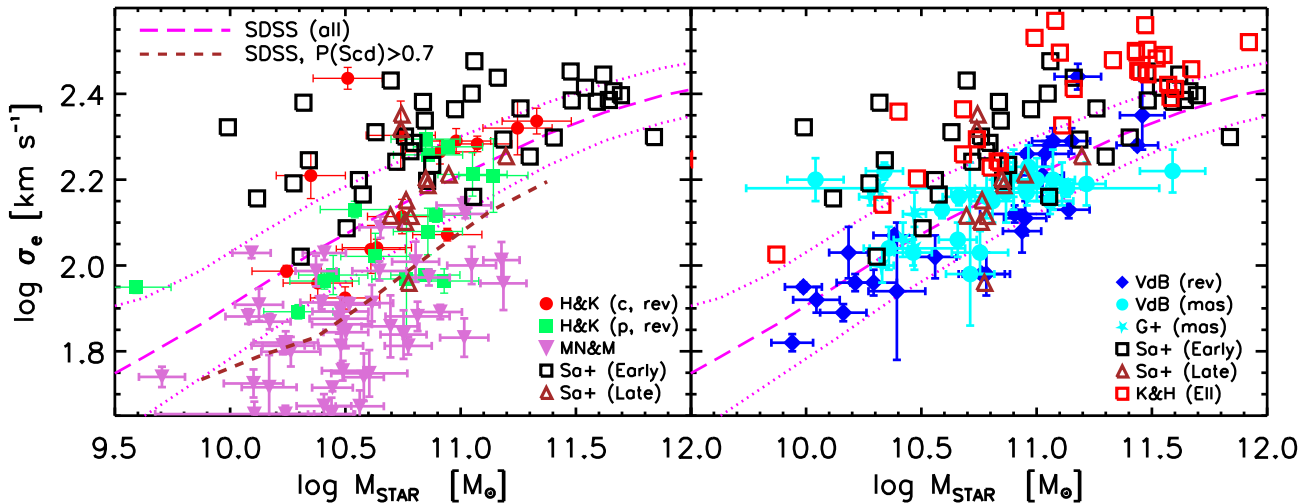
Figure 1. *Left*: Correlation between velocity dispersion and (total) stellar mass in SDSS for all galaxies (long-dashed magenta line; the dotted magenta lines show the region enclosing 68 per cent of the objects at each M_{star}) and also for late-type galaxies with a high probability $P(Scd) > 0.7$ of being classified as late spirals (the brown dashed line). The data are the classical and pseudobulges from Ho & Kim (2014, the red circles and the green squares), and the low-mass Seyferts from Martín-Navarro & Mezcua (2018; the orchid upside down triangles). *Right*: Same correlation between velocity dispersion and (total) stellar mass in SDSS for all galaxies, compared to the reverberation-based and masers from van den Bosch (2016; the blue diamonds and the cyan circles), and the megamasers from Greene et al. (2016; the cyan stars). As in the left-hand panel, the open black squares and the brown triangles are from Savorgnan & Graham (2016), while the open red squares are the elliptical quiescent supermassive black hole sample from Kormendy & Ho (2013). In contrast to the quiescent galaxies, AGN galaxies seem to follow very similar scaling relations to SDSS galaxies. For simplicity, in this and in all subsequent figures, masers are labelled as 'mas', while all other AGN samples with black hole masses based on direct reverberation mapping or reverberation-based (i.e. single-epoch/virial) techniques, are labelled as 'rev'.

still this effect is on average relatively small to account for the full offset. Within the SDSS late-type galaxies, in fact, only Scd galaxies tend to show a moderate offset of ∼0.1 dex in velocity dispersion at fixed stellar mass with respect to the full SDSS galaxy population (left-hand panel). On the other hand, Sab galaxies, which are much more common among (especially Type 1) Seyferts (e.g. Chen & Hwang 2017), share, we checked, a very similar σ–M_{star} relation to the general population.

All in all, from Fig. 1 we conclude that the samples of AGN considered in this work are *not* biased in terms of their velocity dispersions and stellar masses when compared to the SDSS galaxies. In this respect, being more faithful tracers of the local galaxy population, AGN samples appear as a more robust 'training set' to probe the underlying scaling relations between black holes and their host galaxies. The systematic discrepancies, which we will discuss next, between the scaling relations of active and quiescent galaxies in view of Fig. 1 should be mostly ascribed to selections rather than to physical effects. In the framework of the selection effects discussed above, if galaxies are offset in the SDSS σ–M_{star} relation, they should show a higher degree of bias in the M_{bh}–M_{star} relation rather than in the M_{bh}–σ relation. As in fact evidenced from the Monte Carlo simulations (Shankar et al. 2016), selecting sources with larger σ, above the mean σ–M_{star} correlation, would naturally correspond to substantially more massive black holes, due to the steepness and tightness of the underlying M_{bh}–σ relation. At fixed velocity dispersion, the effect of the bias would be less prominent as correlations with the variable on which the selection was made (in this case σ) will naturally be less biased. However, the AGN samples considered in this work, which share a similar σ–M_{star} relation to SDSS galaxies, should present self-consistent black hole scaling relations in terms of velocity dispersion and stellar mass. We will show next that this is indeed the case.

Bentz & Manne-Nicholas (2018) have recently pointed out that the presence of bars in many local galaxies could induce a bias in the SDSS galaxy sample itself. Indeed the number of bars in the SDSS galaxies is significant (e.g. Consolandi 2016). Bars, as also pointed out by Shankar et al. (2016), may increase velocity dispersions at fixed stellar mass (see also Graham et al. 2011 and Batiste et al. 2017). Nevertheless, even if such an effect is present, this would imply an intrinsic/unbiased SDSS σ–M_{star} relation lower in normalization than what plotted in Fig. 1, which would exacerbate the tension with the local sample of black holes in quiescent galaxies. The good match with the AGN hosts tends to either disfavour the presence of a strong bar-induced bias in SDSS galaxies, or points to a similar fraction of barred galaxies among the different samples.

3.2 The M_{bh}–M_{star} relation of local active galaxies

In each panel of Fig. 2, we report the M_{bh}–M_{star} relation from Shankar et al. (2016) of quiescent black holes as extracted from the Savorgnan & Graham (2016) sample with updated black hole masses from Kormendy & Ho (2013), and (total) stellar masses from full bulge–disc decompositions and 3.6 μm mass-to-light ratios $(M/M_\odot)/(L/L_\odot) = 0.6$ from Meidt et al. (2014). The black open squares and the brown triangles represent, as in Fig. 1, early and late-type galaxies, respectively. As discussed in Shankar et al. (2016), we retain from the original Savorgnan & Graham (2016) sample only the galaxies with secure black hole mass measurements and remove those sources classified as ongoing mergers, limiting the final sample to 48 galaxies of which 37 are early-type galaxies (ellipticals or lenticulars). The black long-dashed and dotted lines are the linear fits to the Savorgnan & Graham (2016) early-type and
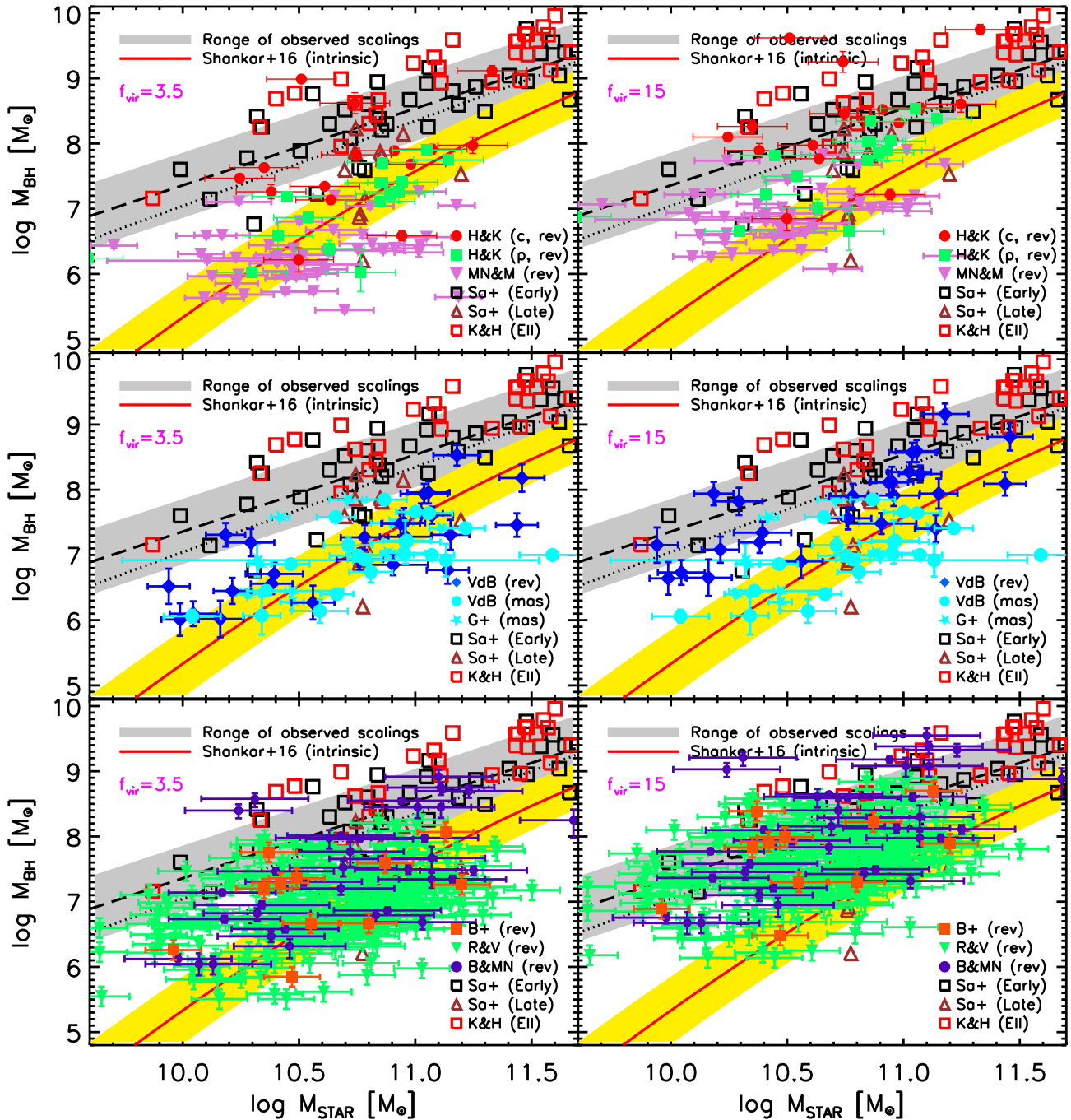
Figure 2. *Left-hand panels*: Correlations between M_{bh}–M_{star} in quiescent galaxies (the black dotted line shows the fit to the all sample; the black dashed line and the grey band show the fit and rms scatter for the early-type quiescent galaxies subsample, respectively) with data from Savorgnan & Graham (2016; the open black squares and the brown triangles) and the ellipticals from Kormendy & Ho (2013; the open red squares), and the unbiased M_{bh}–M_{star} relation predicted by Shankar et al. (2016; the solid red line and the yellow band). The correlations are compared with a variety of samples of active galaxies for which a mean virial factor $f_{vir} = 3.5$ was used. The samples are from Ho & Kim (2014; the red circles and the green squares for classical and pseudobulges, respectively), Martín-Navarro & Mezcua (2018; the orchid upside down triangles), in the top panel, van den Bosch (2016; the blue diamonds and the cyan circles), Greene et al. (2016; the cyan stars), in the middle panel, and Busch et al. (2014; the red squares), Reines & Volonteri (2015; the green upside down triangles), and Bentz & Manne-Nicholas (2018; the purple circles), in the bottom panel. *Right-hand panels*: Same format as left-hand panels but adopting a mean virial factor of $f_{vir} = 15$ for all virial-based active black hole mass measurements. When adopting the mean virial factor of $f_{vir} = 3.5$ as constrained by Grier et al. (2017), most of the active galaxies tend to better line up with the Shankar et al. (2016) 'intrinsic/unbiased' M_{bh}–M_{star} relation (left-hand panels), while substantially larger virial factors are required to match the M_{bh}–M_{star} relation of quiescent galaxies (right-hand panels).

full sample, respectively,

$$\log \frac{M_{\rm bh}}{M_\odot} = 8.54 + 1.18 \log \left(\frac{M_{\rm star}}{10^{11} M_\odot} \right) \tag{3}$$

and

$$\log \frac{M_{\rm bh}}{M_\odot} = 8.35 + 1.31 \log \left(\frac{M_{\rm star}}{10^{11} M_\odot} \right), \tag{4}$$

while the grey area (corresponding to a scatter of 0.5 dex) broadly brackets the uncertainty region around the observed $M_{\rm bh}$–$M_{\rm star}$ observed in local early-type quiescent galaxies. For completeness, we also plot the elliptical galaxies from the original Kormendy & Ho (2013; the open red squares) sample, which all lie within, if not even above, the grey band. We indeed verified that all the local quiescent black hole samples considered by Shankar et al. (2016) fall within the grey band.

The solid red line is instead the intrinsic/unbiased (or de-biased) black hole mass versus total stellar mass ($M_{\rm bh}$–$M_{\rm star}$) relation proposed by Shankar et al. (2016):

$$\log \frac{M_{\rm bh}}{M_\odot} = 7.574 + 1.946 \log \left(\frac{M_{\rm star}}{10^{11} M_\odot} \right) - 0.306 \tag{5}$$
$$\times \left[\log \left(\frac{M_{\rm star}}{10^{11} M_\odot} \right) \right]^2 - 0.011 \left[\log \left(\frac{M_{\rm star}}{10^{11} M_\odot} \right) \right]^3,$$

with a mass-dependent intrinsic scatter (yellow region) given by

$$\Delta \log \frac{M_{\rm bh}}{M_\odot} = 0.32 - 0.1 \times \log \left(\frac{M_{\rm star}}{10^{12} M_\odot} \right). \tag{6}$$

(equation 5 is applicable to galaxies with stellar mass above $\log M_{\rm star}/M_\odot > 10$). The Shankar et al. (2016) relation (labelled as 'intrinsic') is significantly lower in normalization and steeper than the relation that would be inferred by directly fitting the Savorgnan & Graham (2016) data (the long-dashed and dotted lines). This different shape in the intrinsic $M_{\rm bh}$–$M_{\rm star}$ relation mainly reflects the curvature in the σ–$M_{\rm star}$ relation (Fig. 1), and the fact that the black hole mass is tightly related to velocity dispersion. We note that, strictly speaking, the unbiased relation put forward by Shankar et al. (2016) has been calibrated against the SDSS early-type galaxies, and thus it should be preferentially compared to the black long-dashed line. Nevertheless, late-type galaxies become progressively subdominant at stellar masses $\log M_{\rm star}/M_\odot \gtrsim 10.5$ (e.g. Bernardi et al. 2013), and if included they would tend, if anything, to decrease the mean velocity dispersions by $\lesssim 0.05$ dex at the stellar masses considered in this work. In turn, the unbiased $M_{\rm bh}$–$M_{\rm star}$ relation would then be proportionally lower at fixed host stellar mass, thus further increasing the mismatch with the scaling relation of quiescent galaxies. In what follows, we will thus continue to safely consider the yellow band as the region encompassing the intrinsic $M_{\rm bh}$–$M_{\rm star}$ relation of the full local central black hole population hosted in relatively massive galaxies.

It should be noted that in Fig. 2 we include all the AGN data sets detailed in Appendix A. In the upper panels, we include the classical and pseudobulges reverberation-based black hole masses from Ho & Kim (2014; the filled red circles and the green squares, respectively) and the low-mass Seyferts from Martín-Navarro & Mezcua (2018; the orchid upside down triangles), in the middle panels the megamasers from Greene et al. (2016; the filled cyan stars), and the virial-based (i.e. single epoch) and masers AGN from van den Bosch (2016; the blue diamonds and the cyan circles for reverberation-based and masers AGN, respectively), and in the lower panels the virial-based black holes in low-luminosity quasars

from Busch et al. (2014; the red filled squares), the virial-based AGN from Bentz & Manne-Nicholas (2018; the purple circles), and the SDSS virial-based AGN from Reines & Volonteri (2015; the green upside down triangles).

It is clear from the left-hand panels of Fig. 2 that when adopting a uniform virial factor of $f_{\rm vir} = 3.5$, as independently calibrated by Grier et al. (2017) and Williams et al. (2018) via direct BLR modelling, the vast majority of the data tend to lie on average within the yellow band of Shankar et al. (2016). However, we stress that the latter is *not* a fit to the AGN samples. Indeed, some of the data sets present larger scatter than what implied by the yellow band, as evident, for example, in the Martín-Navarro & Mezcua (2018) and Reines & Volonteri (2015) sources. The Reines & Volonteri (2015) and van den Bosch (2016) samples also tend to be better fitted by a linear relation between black hole and stellar mass, somewhat flatter than the nearly quadratic one suggested by equation (5). On the other hand, the Bentz & Manne-Nicholas (2018) sources are consistent with a similarly steep relation. It is worth noticing that some among the most massive ($M_{\rm star} \gtrsim 10^{11}$ M$_\odot$) sources in Bentz & Manne-Nicholas (2018) lie above equation (5), lining up with the observed $M_{\rm bh}$–$M_{\rm star}$ relation, though, however, the sample taken as a whole still points to an average lower $M_{\rm bh}$–$M_{\rm star}$ scaling relation. We note that Bentz & Manne-Nicholas (2018)'s choice of limiting the Sérsic index to $n_{\rm Ser} \leq 4$ could lead to underestimate the luminosities of their most massive galaxies, which are usually characterized in SDSS by progressively higher Sérsic indices (e.g. Bernardi et al. 2014). In this respect, it is worth stressing that all the galaxies in the Busch et al. (2014) sample, which is a mixture of early- and late-type galaxies, all lie significantly below the observed scaling relations.

An average virial factor of $f_{\rm vir} = 3.5$ seems insufficient to reconcile active black holes to the scaling relations observed for quiescent black holes (the black lines). As shown in the right-hand panels of Fig. 2, we would in fact need to increase the virial factor by more than an order of magnitude, e.g. $f_{\rm vir} \gtrsim 15$, in order to be roughly consistent with the observed $M_{\rm bh}$–$M_{\rm star}$ relations (the black dotted and long-dashed lines), at least around $\log M_{\rm star}/M_\odot \gtrsim 11$. At lower stellar masses, the AGN data would require even higher virial factors due to the stronger steepness of their $M_{\rm bh}$–$M_{\rm star}$ relation. A more quantitative analysis of the appropriate virial factors needed to match the scaling relations of quiescent black holes will be presented in Section 3.4.

It is worth noticing that when increasing the virial factor only the virial-based black hole masses are proportionally varied but not the ones based on independent maser measurements. This creates a systematic discrepancy that is evident in the middle, right-hand panel of Fig. 2 between the masers by Greene et al. (2016; the cyan stars) and van den Bosch (2016; the cyan circles) with the virial-based black holes from the same van den Bosch (2016; the blue diamonds) sample. This offset is not present when $f_{\rm vir} = 3.5$ is adopted (middle left-hand panel), thus lending further support to the presence of a bias in inactive black holes.

Last but not the least, in line with local quiescent black holes, all the AGN data sets considered in this work lack low black hole masses in massive hosts. The existence of a finite (though possibly large) scatter in the local scaling relations supports the view of an underlying black hole-host galaxy correlation (a 'ridge' as labelled by Shankar et al. 2016), and disfavours the idea that local black hole-host scaling relations mark the upper envelope of a uniform distribution of black hole masses (e.g. Batcheldor 2010).

3.3 The M_{bh}–σ relation of local active galaxies

In Fig. 3, we present a similar comparison between quiescent and active galaxies as in Fig. 2 but for the M_{bh}–σ relation. The open black squares and the brown triangles are the early and late galaxies by Savorgnan & Graham (2016) with velocity dispersions originally taken from Hyperleda data base (Paturel et al. 2003) with a nominal aperture of 0.595 kpc. We thus correct via equation (A3) all their velocity dispersions to an aperture equal to one effective radius, with effective radii also self-consistently measured by Savorgnan & Graham (2016). A direct linear fit (see appendix A in Shankar et al. 2017) to the quiescent early-type sample yields (the black long-dashed line):

$$\log \frac{M_{bh}}{M_\odot} = 8.51 + 5.09 \left(\log \frac{\sigma_e}{km\,s^{-1}} - 2.3 \right), \qquad (7)$$

with a scatter around ~0.4 dex (grey region). Equation (7) is close in both slope and normalization to equation (5) in Kormendy & Ho (2013). The fit to the early-type black hole population is very similar (the black long-dashed line) as both early- and late-type galaxies are less scattered in the M_{bh}–σ relation (e.g. van den Bosch 2016, and references therein). The Monte Carlo simulations by Shankar et al. (2016) have revealed that assuming an underlying basic selection bias in the gravitational sphere of the central black hole yields an observed M_{bh}–σ offset from the intrinsic/unbiased one by ~0.5 dex but with a similar slope, if the intrinsic scatter is $\lesssim 0.3$ dex (their fig. 9). For our reference intrinsic/unbiased M_{bh}–σ relation we thus choose to adopt equation (7) simply lowered in normalization by 0.5 dex (the solid red line and the yellow region). For completeness, as in previous figures, we also report in Fig. 3 the elliptical sample of Kormendy & Ho (2013; the open red triangles) that is fully consistent with the observed M_{bh}–σ relation from the Savorgnan & Graham (2016) sample of quiescent galaxies (the black lines).

Following the format of Fig. 2, retaining the AGN samples for which we have published velocity dispersions, in the upper panels of Fig. 3 we include the classical and pseudobulges reverberation-based black holes from Ho & Kim (2014; the filled red circles and the green squares, respectively) and the virial-based low-mass Seyferts from Martín-Navarro & Mezcua (2018; the orchid upside down triangles), in the lower panels the megamasers from Greene et al. (2016; the filled cyan stars), and the virial-based black holes and masers from van den Bosch (2016; the blue diamonds and the cyan circles for reverberation-based and masers AGN, respectively). In the left-hand panels, we assume a uniform virial factor $f_{vir} = 3.5$ and $f_{vir} = 8$ in the right-hand panels. It is evident that, at least for galaxies with velocity dispersions above $\log \sigma / km\,s^{-1} \gtrsim 1.9$, the former provides a better match to the unbiased relation, while the latter to the observed relation. More quantitative estimates of the appropriate virial scaling factors are given in Section 3.4. Above $\log \sigma / km\,s^{-1} \gtrsim 1.9$, active black holes tend to follow a M_{bh}–σ relation similar in slope to the quiescent samples, in line with what also claimed by Woo et al. (2013b). At lower velocity dispersions, below $\log \sigma / km\,s^{-1} \lesssim 1.9$, the Martín-Navarro & Mezcua (2018; the orchid upside down triangles in the upper panels) sample tends to flatten out, as already noted by Martín-Navarro & Mezcua (2018), and also tends to become more scattered. Baldassare et al. (2016) on the other hand found that the lowest mass galaxies with AGN signatures in their sample fall within the extrapolations of the M_{bh}–σ of quiescent black holes. The main conclusions of this work anyway hold for galaxies with $\log \sigma / km\,s^{-1} \gtrsim 1.9$, i.e. with stellar masses $\log M_{star}/M_\odot \gtrsim 10$ according to the mean σ–M_{star} relation of SDSS

galaxies (the long-dashed line in Fig. 1). The data on both active and quiescent galaxies become much more sparse below this threshold.

3.4 A distinct virial factor f_{vir} for the observed M_{bh}–M_{star} and M_{bh}–σ relations

In the previous sections, we found that assuming an underlying virial factor of $f_{vir} = 3.5$ provides a reasonable match to both the unbiased M_{bh}–M_{star} and M_{bh}–σ relations put forward by Shankar et al. (2016). On the other hand, larger values of f_{vir} are required to broadly match the observed scaling relations of black holes in quiescent galaxies. In particular, there is evidence for the need of a particularly large f_{vir} when comparing with the observed M_{bh}–M_{star} relation (right-hand panels of Fig. 2). In Fig. 4, we provide a more thorough investigation into the distributions of virial factors f_{vir} required to match both the observed (upper panels) and unbiased (lower panels) relations. For this purpose, we choose the two reverberation-based data sets of classical/pseudobulges by Ho & Kim (2014; the red solid lines) and the virial-based AGN by van den Bosch (2016; the long-dashed lines). Both samples share a broad coverage in stellar mass and velocity dispersion, and are not biased with respect to the σ–M_{star} relation of SDSS galaxies (Fig. 1). For each AGN sample and a given input f_{vir}, we then perform a linear fit to the M_{bh}–σ and M_{bh}–M_{star} relations and compute their offsets with respect to the analogous relations for quiescent galaxies. Our methodology, which is slightly different from the one put forward by, e.g. Onken et al. (2004, their equation 3), allows to determine the offsets between the active and quiescent populations in a given bin of stellar mass or velocity dispersion, particularly relevant when the slopes tend to be different, as in the M_{bh}–M_{star} plane (Fig. 2).

The left-hand panels of Fig. 4 show the displacement in $\log M_{bh}$ between the $\log M_{bh}$–$\log M_{star}$ relation of quiescent and active galaxies computed at $\log M_{star}/M_\odot = 11$ as a function of the virial factor f_{vir}. Both samples suggest that, in agreement with Fig. 2, only virial factors $f_{vir} \gtrsim 15$ tend to align the AGN with the quiescent galaxies within $\Delta \log M_{bh} \lesssim 0.1$ dex in the M_{bh}–M_{star} relation. The reference virial factor of $f_{vir} = 3.5$ (the vertical magenta dotted lines in Fig. 4), in particular, would generate an offset of $\Delta \log M_{bh} \sim 0.8$ dex, in order for the reverberation/virial-based AGN to line up to the relation observed in quiescent ellipticals. Note that we deliberately chose to compute the displacements at relatively high stellar masses $\log M_{star}/M_\odot = 11$ as at lower masses the match would require even higher f_{vir} to bring AGN in line with the relation of quiescent galaxies, being the former steeper than the latter (see Section 3.2). In the right-hand panels of Fig. 4, we instead plot as a function of the virial factor f_{vir} the displacement in $\log M_{bh}$ between the $\log M_{bh}$–$\log \sigma$ relation of quiescent and active galaxies computed at $\log \sigma / km\,s^{-1} = 2.2$, which is the mean velocity dispersion roughly corresponding to $\log M_{star}/M_\odot = 11$, following the SDSS σ–M_{star} relation (Fig. 1). In this case the match between AGN and quiescent galaxies within $\Delta \log M_{bh} \lesssim 0.1$ dex in the M_{bh}–σ relation is reached for $f_{vir} \gtrsim 7$, roughly a systematic factor of two lower than the f_{vir} required to match the M_{bh}–M_{star} relation.

This systematic difference in virial factors can be easily interpreted within, and in fact taken in support of, the framework of the selection bias considered by Shankar et al. (2016). As discussed with respect to Fig. 1, this bias induces the selection of sources with velocity dispersions on average higher than regular counterpart SDSS galaxies of similar stellar mass. In turn, higher velocity dispersions would imply selecting on average higher mass black holes, given the strong dependence $M_{bh} \propto \sigma^{4-5}$. Ultimately, this
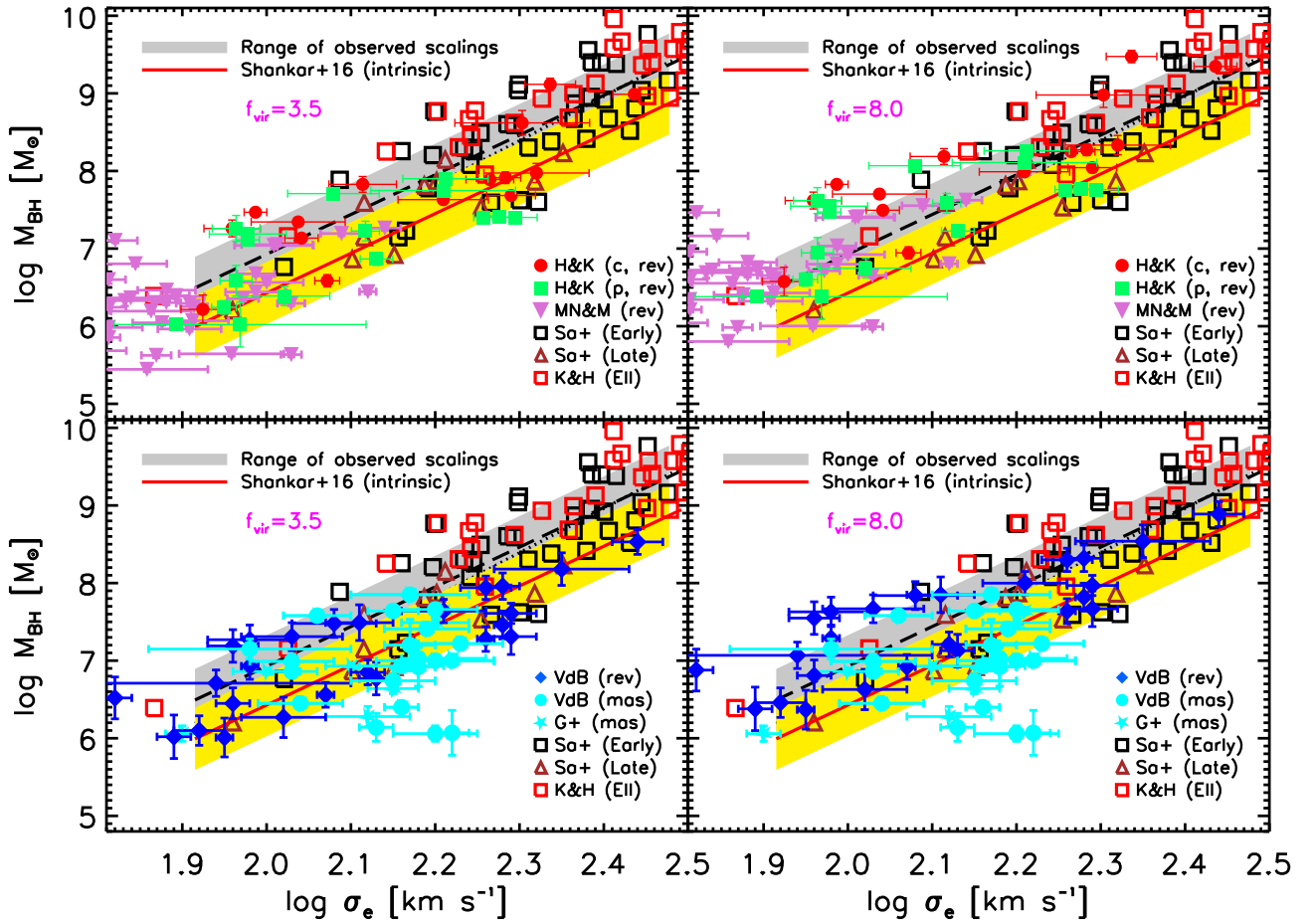
Figure 3. Same format as Fig. 2 but for the correlations between M_{bh}–σ in the Savorgnan & Graham (2016) quiescent galaxies (the black lines and the grey band) and the 'intrinsic' (unbiased) M_{bh}–σ relation predicted by Shankar et al. (2016; the solid red line and the yellow band). When adopting the mean virial factor of $f_{vir} = 3.5$ as constrained by Grier et al. (2017), most of the data tend to better line up with the Shankar et al. (2016) 'intrinsic/unbiased' M_{bh}–σ relation (left-hand panels), while substantially larger virial factors are required to match the M_{bh}–σ relation of quiescent galaxies (right-hand panels). More quantitative estimates of the appropriate virial scaling factors are given in Fig. 4.

selection bias is expected to artificially increase the normalization of the black hole scaling relations, in particular of the M_{bh}–M_{star} relation, which is a direct reflection of the σ–M_{star} relation. In practice, the presence of such a bias requires a mean f_{vir} factor systematically higher, by at least a factor of 2, in the M_{bh}–M_{star} than in the M_{bh}–σ relation. On the other hand, the *same* virial factors of $f_{vir} \sim 3$–4 are consistent with both the intrinsic relations within $\lesssim 0.1$ dex uncertainty (bottom panels of Fig. 4). An $f_{vir} \sim 3$–4 also does not show the discrepancy between the masers and the reverberation-based black holes, which appears instead when a higher f_{vir} is adopted (compare the cyan stars and the cyan circles in the middle, right-hand panel of Fig. 2).

3.5 Residuals in the active black hole scaling relations

It has been discussed by a number of groups (Bernardi et al. 2007; Shankar et al. 2016; van den Bosch 2016; Barausse et al. 2017; Shankar et al. 2017) that velocity dispersion is a galactic property linked to black hole mass more fundamentally in terms of residuals than any other one, including stellar/bulge mass, light profile concentration, or effective radius. Residuals in pairwise correlations (Sheth & Bernardi 2012) are in fact an effective methodology to probe underlying relations among variables. The left-hand and right-

hand panels of Fig. 5 report the $\Delta(M_{bh}|M_{bulge})$ versus $\Delta(\sigma|M_{bulge})$ and $\Delta(M_{bh}|\sigma)$ versus $\Delta(M_{bulge}|\sigma)$, where

$$\Delta(Y|X) \equiv \log Y - \langle \log Y \,|\, \log X \rangle \qquad (8)$$

is the residual in the Y variable (at fixed X) from the log–log linear fit of $Y(X)$ versus X, i.e. $\langle \log Y | \log X \rangle$.

For this test, analogously to what was performed in Fig. 4, we use the reverberation-based Ho & Kim (2014) and virial-based van den Bosch (2016) samples that share a broad coverage in stellar mass and velocity dispersion and are not biased with respect to the σ–M_{star} relation of SDSS galaxies. For the Ho & Kim (2014) sample, in particular, we show results using *bulge* rather than total stellar masses, being the former more physically related to central velocity dispersion. We assume a constant $f_{vir} = 3.5$ for all sources in both samples. To produce residuals, we follow the procedure outlined in Shankar et al. (2016) and Shankar et al. (2017). For each residual we run 200 iterations, and at each iteration we eliminate two random objects from the original sample. From the full ensemble of realizations, we measure the mean slope and its 1σ uncertainty.

Fig. 5 clearly shows that black hole mass is strongly correlated with velocity dispersion at fixed bulge stellar mass with a Pearson coefficient $r = 0.65$ (top left-hand panel), while the correlation with bulge mass is negligible with $r = 0.16$ at fixed velocity
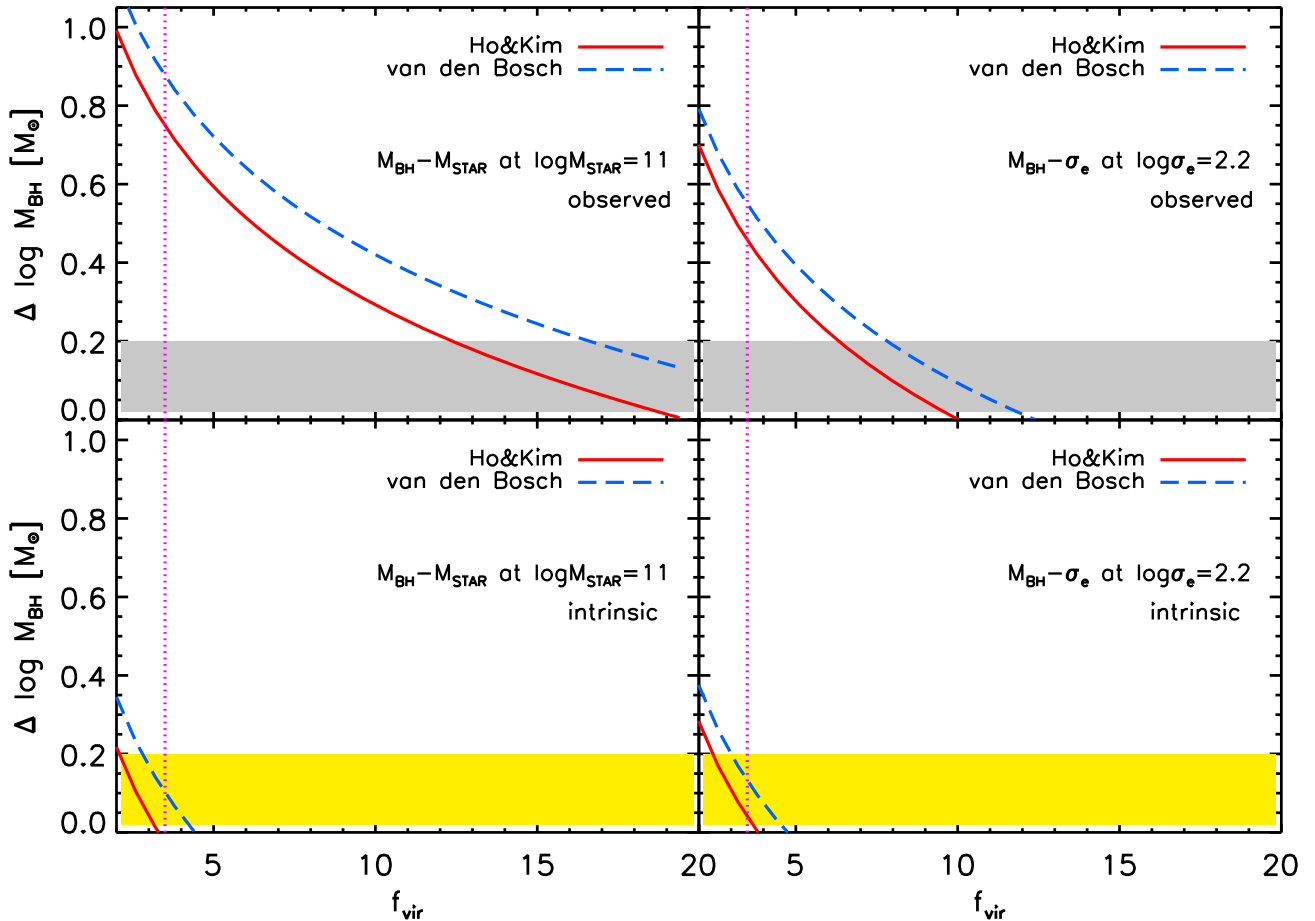
Figure 4. *Left*: Displacement in $\log M_{bh}$ between the $\log M_{bh}-\log M_{star}$ relation of quiescent and active galaxies computed at $\log M_{star}/M_\odot = 11$ as a function of the virial factor f_{vir}. *Right*: Displacement in $\log M_{bh}$ between the $\log M_{bh}-\log \sigma$ relation of quiescent and active galaxies computed at $\log \sigma/\mathrm{km\,s^{-1}} = 2.2$ as a function of the virial factor f_{vir}. The solid red and long-dashed blue lines refer to the sample of Ho & Kim (2014) and van den Bosch (2016; only reverberation-based AGN), as labelled. The top and lower panels adopt the observed (the grey band) and unbiased (the yellow bands) black hole relations shown in Figs 2 and 3, respectively. The required virial factors are in general large for the observed relations ($f_{vir} > 6$). For the $\log M_{bh}-\log M_{star}$ relation the f_{vir} factor is systematically higher by at least a factor of 2, as expected in the presence of a bias in the sample of quiescent galaxies. The same virial factors of $f_{vir} \sim 3-5$ are instead consistent with the de-biased relations within $\lesssim 0.1$ dex uncertainty (see text for details). The vertical magenta dotted lines mark the reference virial factor of $f_{vir} = 3.5$.

dispersion (top right-hand panel). When computing residuals for only classical bulges (the red circles, middle panels), the correlation with velocity dispersion becomes even more marked with a Pearson coefficient of $r = 0.74$, while the one with bulge mass further decreases to $r = 0.13$. Adopting total stellar masses in the Ho & Kim (2014) sample and/or their original values for f_{vir} would produce even stronger residuals with velocity dispersion, further corroborating our results. The lower panels of Fig. 5 show that the residuals extracted from the reverberation-based sample from van den Bosch (2016) still point to strong correlation with velocity dispersion ($r = 0.68$) and a negligible one with (total) stellar mass ($r = 0.06$).

These findings fully confirm and extend to local AGN the dominance of velocity dispersion in pairwise scaling relations put forward by Bernardi et al. (2007) and Shankar et al. (2016) for local quiescent black holes. The total slope of the $M_{bh}-\sigma$ relation in AGN can be estimated as $M_{bh} \propto \sigma^\beta M_{star}^\alpha \propto \sigma^{\beta+\alpha\gamma}$, where γ comes from $M_{star} \propto \sigma^\gamma$. Since SDSS galaxies tend towards $\gamma \approx 2.2$ (Shankar et al. 2017), and the residuals in Fig. 5 yield $\beta \sim 4-5$ and $\alpha \sim 0.1-0.2$, one obtains a total dependence of $M_{bh} \propto \sigma^{4.2-5.5}$,

consistent with models of black hole growth being regulated by energy/momentum-driven AGN feedback (e.g. Silk & Rees 1998; Fabian 1999; King 2003; Granato et al. 2004).

4 DISCUSSION AND CONCLUSIONS

The first result of this work is that the samples of local ($z < 0.3$) AGN considered here with measured velocity dispersions and stellar masses are consistent, on average, with those from the SDSS galaxies (Fig. 1). This is in stark contrast to samples of quiescent black holes, which are biased with respect to the full SDSS sample (Bernardi et al. 2007; Shankar et al. 2016). The second result concerns the factor f_{vir} that is adopted to normalize black hole masses in reverberation-based AGN samples (e.g. Peterson 1993). Values of order $f_{vir} \sim 15$ are required to match the selection-biased $M_{bh}-M_{star}$ relation of quiescent galaxies, whereas $f_{vir} \sim 3.5$, as derived from direct modelling of the BLR (e.g. Williams et al. 2018, and references therein), is required to match the Shankar et al. (2016)'s estimate of the intrinsic relation for quiescent galaxies (Fig. 2). Water masers, with black hole masses independent of any
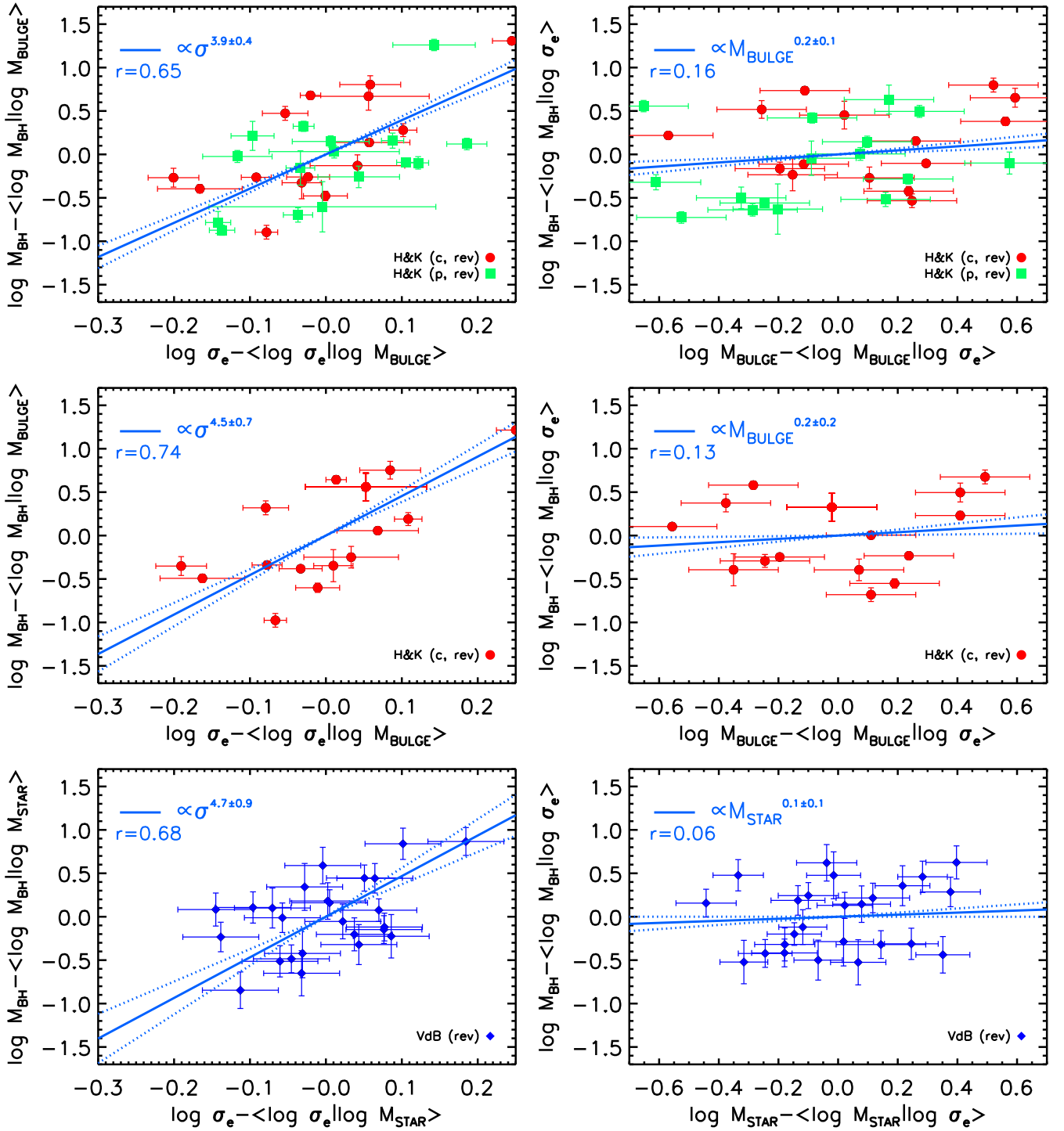
Figure 5. Correlations between residuals from the observed scaling relations, as indicated. The red circles and the green squares in the top panels show, respectively, classical and pseudobulges from Ho & Kim (2014). The middle panels show the subsample of classical bulges. The blue filled diamonds in the bottom panels are the reverberation-based data from van den Bosch (2016). Correlations with velocity dispersion appear to be much stronger (left-hand panels; Pearson coefficient $r \sim 0.6-0.7$) than those with bulge/total stellar mass (right-hand panels; $r \lesssim 0.1-0.2$), in line with that observed for local samples of quiescent supermassive black holes with dynamical mass measurements.

virial factor, also fall within the scatter of the unbiased relations by Shankar et al. (2016, the cyan symbols in Figs 2 and 3).

A number of other groups had also found significant discrepancies between AGN samples, with virial factors f_{vir} calibrated against some renditions of the $M_{bh}-\sigma$ relation, and the observed $M_{bh}-M_{star}$

relation of quiescent black holes (e.g. Dasyra et al. 2007; Kim et al. 2008; Sarria et al. 2010; Busch et al. 2014; Falomo et al. 2014; Reines & Volonteri 2015; Greene et al. 2016; Bentz & Manne-Nicholas 2018), though without offering a convincing explanation for the nature of this puzzling offset. Reines & Volonteri (2015),

in particular, carried out a detailed work to compare one of the largest local samples of broad-line AGN (244 sources) with virial black hole mass estimates, with the samples of quiescent galaxies from Kormendy & Ho (2013), as (re)proposed in the bottom panels of our Fig. 2. After applying appropriate corrections to different total stellar mass estimates, they concluded that the substantial discrepancy ($\sim$1.2 dex) in the normalization between the active and quiescent samples cannot be ascribed to only measurement errors. Indeed, they found that reconciling the two samples would require average virial factors of the order of $f_{\rm vir} \gtrsim 40$, which is significantly beyond the typical uncertainties in $f_{\rm vir}$. Bennert et al. (2011) also found evidence for a mean discrepancy between local active and inactive galaxies in terms of spheroidal luminosity (upper left-hand panel of their fig. 17), though it tends to disappear when converting to stellar masses (middle upper panel of their fig. 17) most probably due to their specific choices of mass-to-light ratios.

We are thus not the first to report on an apparent discrepancy between scaling relations of active and quiescent local black hole samples (e.g. Reines & Volonteri 2015). However, our work offers new insights into the origin of this discrepancy. In particular, it highlights the important role played by angular resolution-related selection effects on the quiescent sample. We showed in fact that the mean $f_{\rm vir}$ required to match the selection-based $M_{\rm bh}$–$M_{\rm star}$ relation of quiescent black holes is systematically higher by a factor $\sim$2$-$3 than that needed to match the $M_{\rm bh}$–σ relation. However, once the selection effect has been accounted for, values of $f_{\rm vir} \sim 3.5$ yield agreement with both relations. Ho & Kim (2014) also found evidence for a systematic difference in virial factors. They claimed that classical, more massive bulges required $f_{\rm vir} \sim 6.3$ to match the $M_{\rm bh}$–σ relation of Kormendy & Ho (2013), and a virial factor of $f_{\rm vir} \sim 9$ ($\sim$0.4 dex higher) to match the $M_{\rm bh}$-$M_{\rm bulge}$ relation.

Previously, before the black hole mass revisions outlined in Kormendy & Ho (2013, and references therein), lower values of the $f_{\rm vir}$ factors had been reported in the literature (see Section 1). For example, when comparing to the Woo et al. (2013a) $M_{\rm bh}$–σ relation of quiescent black holes, Grier et al. (2013) retrieved a mean $f_{\rm vir} \sim 4.3$. Shankar et al. (2016) reported that mean virial factors calibrated on the observed $M_{\rm bh}$–σ relation should be reduced by a factor of $\sim$3 to account for selection bias (see also Fig. 3). They thus suggested that the mean virial factor could be of order unity based on the Grier et al. (2013) estimate of $f_{\rm vir} \sim 4$. However, we here showed, in broad accordance with Ho & Kim (2014), that a more proper comparison with the most recent scaling relations of quiescent black holes suggests $f_{\rm vir} \sim 10$$-$12 for a close match to the $M_{\rm bh}$–σ relation (upper right-hand panel of Fig. 3), which would then imply a scaled $f_{\rm vir} \sim 3.5$$-$4 to match the unbiased relation (left-hand panels of Fig. 3), in nice agreement with the independent estimate of $f_{\rm vir} \sim 3.5$ by, e.g. Grier et al. (2017) and Williams et al. (2018). Finally, the correlation between $M_{\rm bh}$–$M_{\rm star}$ of the masers is more consistent with that of the reverberation-based black holes if a $f_{\rm vir} \sim 3$$-$4 is adopted instead of a higher value.

It is very unlikely, also given the great diversity of AGN samples collected here, that the observed large offsets in black hole mass with respect to the observed relations of local quiescent black holes is a mere consequence of 'infant' black holes still growing towards their final mass (e.g. Mathur et al. 2012), especially in the local Universe, vastly dominated by AGN with low characteristic Eddington ratios (e.g. Kauffmann & Heckman 2009; Shankar, Weinberg & Miralda-Escudé 2013). These findings instead lend further support to the presence of a strong bias in the local quiescent black hole sample, possibly caused by the limited telescope resolution power that artificially increases the normalization of the σ–$M_{\rm star}$ relation along

with other scalings (e.g. Bernardi et al. 2007; Shankar et al. 2016, 2017). This bias has important consequences on a number of fronts, from implications for seeds and intermediate mass black holes (e.g. Graham 2016; Shankar et al. 2016; Mezcua 2017; Pacucci et al. 2018), gravitational waves (e.g. Sesana et al. 2016; Taylor, Simon & Sampson 2017; Chen, Sesana & Conselice 2018; Joshi et al. 2018), to radiative/kinetic efficiencies (Shankar et al. 2019, submitted).

Reines & Volonteri (2015) pointed out that the quiescent subsample of late-type galaxies, especially pseudobulges, with dynamically measured black holes tends to overlap with the black hole scaling relations in active galaxies. We do find a similar trend with the (few) late-type galaxies in the Savorgnan & Graham (2016) sample overlapping with our intrinsic black hole scaling relations (Figs 2 and 3). In our interpretation, the displacement, or lack thereof, between the relations of active and quiescent black holes can be explained by how much the host galaxies are outliers in the SDSS σ–$M_{\rm star}$ relation (Fig. 1). Late-type galaxies, usually characterized by lower velocity dispersions at fixed stellar mass, will always be less biased than early-type galaxies, thus naturally appearing more consistent with the intrinsic scaling relations of black holes.

We stress that all the results presented here, including equations (5) and (7), are mostly applicable to galaxies with (total) stellar mass $\log M_{\rm star}/M_\odot \gtrsim 10$ and velocity dispersion $\log \sigma/{\rm km\,s}^{-1} \gtrsim 1.9$. Although our AGN samples and SDSS data become rapidly more sparse and/or less robust below this limit, some efforts to probe black hole scaling relations at lower stellar masses have been attempted in recent years. Graham, Soria & Davis (see e.g. 2019, and references therein) suggest that a steepening should be present in the $M_{\rm bh}$–$M_{\rm star}$ relation at low stellar masses, while a flattening in the $M_{\rm bh}$–σ relation seems to be more consistent with the data according to Martín-Navarro & Mezcua (2018) and Fig. 3 (but see also Baldassare et al. 2016). In the context of further probing the correlations of active black holes at lower stellar masses, we also considered six low-mass galaxies from the SDSS-IV Mapping Nearby Galaxies with AGN signatures (Penny et al. 2018). We computed stellar masses for these galaxies from their $r - i$ colours and the mass-to-light ratios from Bell et al. (2003b), decreased by 0.1 dex to convert to a Chabrier IMF. Velocity dispersion were corrected to an aperture of one effective radius using equation (A3), in which the Sérsic index was set to $n_{\rm Ser} = 2$ (this choice does not have any impact on our results). Black hole masses were then inferred from equation (7) lowered by 0.5 dex to convert to the intrinsic $M_{\rm bh}$–σ. We found the median black hole mass competing to a median host stellar mass of $\log M_{\rm star}/M_\odot \sim 9.7$, to be $\log M_{\rm bh}/M_\odot \sim 5.3$, which should be regarded more as an upper limit, as three galaxies have only assigned upper limits to their velocity dispersions. The median black hole mass in these dwarfs lies nicely within the 1σ of the intrinsic $M_{\rm bh}$–$M_{\rm star}$ relation reported in Fig. 3. We have also compared with the sample of dwarfs included in table 3 of Reines & Volonteri (2015), which yield, once converted to our reference mass-to-light ratio via equation (A1), a mean black hole mass of $\log M_{\rm bh}/M_\odot \sim 5.6 \pm 0.5$ at $\log M_{\rm star}/M_\odot \sim 9.7$. The latter sample of dwarfs is $\sim 2\sigma$ above the extrapolation of equation (5), possibly suggesting that a drop in black hole masses as marked as predicted by the *extrapolation* of our equation (5) may be inconsistent with present data. In any event, probing the $M_{\rm bh}$–$M_{\rm star}$ correlation at such low stellar masses falls beyond the parameter space probed by the Monte Carlo simulations performed by Shankar et al. (2016), which, as already stressed above, were based on relatively massive galaxies with $\log M_{\rm star}/M_\odot \gtrsim 10$. What is more relevant to emphasize in the context of this paper is that all the dwarfs considered here fall an order of magnitude of more below

the extrapolation of the *observed* M_{bh}–M_{star} relation of quiescent black holes (the grey region in Fig. 2).

It is relevant to note that most of the data adopted here are extracted from samples of Type 1 AGN. We note, however, that recent work has proven Type 2 AGN to be characterized, if anything, by even lower scaling relations (e.g. Ricci et al. 2017a), which would further strengthen our claim for a bias in the M_{bh}–M_{star} relation of dynamically measured quiescent supermassive black holes.

We have finally investigated into AGN samples at higher redshifts, with stellar masses/black hole masses derived from spectral energy decomposition analysis and single epoch spectroscopy (e.g. Chang et al. 2017; Delvecchio et al. 2017; Rowan-Robinson et al. 2017). In all cases, we find the black holes to lie substantially below the local observed M_{bh}–M_{star} relation. However, probing the presence of biases in the M_{bh}–M_{star} relation at higher redshifts becomes increasingly less robust due to the possibility of sampling growing black holes, and/or due to intrinsic evolutionary effects in the M_{bh}–M_{star} relation itself, and/or due to severe flux limitations (e.g. Bongiorno et al. 2014). To conclude, in this work we showed that

(i) AGN hosts follow the σ–M_{star} correlation of SDSS galaxies, in stark contrast to quiescent galaxies with dynamical mass measurements of their black holes (Fig. 1). This behaviour can be in large part explained by the selection effect imposed on the sample of quiescent galaxies by the limited telescope resolution power, which forces to preferentially target more massive, larger velocity dispersions black holes to allow for resolved dynamical mass modelling.

(ii) When adopting mean virial factors of $f_{vir} = 3.5$ from direct modelling of the BLR, distinct data sets of local active galaxies with accurate galaxy mass measurements all point to a M_{bh}–M_{star} relation steeper and with a much lower normalization than the selection biased one observed for local quiescent black holes with dynamical mass measurements (Fig. 2).

(iii) The same data sets of local active galaxies with also available velocity dispersion measurements, all point to a M_{bh}–σ relation, at least at $\log \sigma / \mathrm{km\,s^{-1}} \gtrsim 1.9$, with a similar slope but offset by a factor of ~ 3 from the selection biased one observed for local quiescent black holes with dynamical mass measurements (Fig. 3).

(iv) The mean virial factors required for the AGN samples with reverberation-based black hole measurements to match the high-mass end of, respectively, the M_{bh}–σ and M_{bh}–M_{star} relations of quiescent galaxies within $\lesssim 0.1$ dex accuracy are $f_{vir} \gtrsim 7$ and $f_{vir} \gtrsim 15$, substantially higher than the canonical $f_{vir} \sim 3.5$ (Fig. 4). This systematic offset in f_{vir} can be naturally explained within the framework of the same selection effects in the local sample of quiescent black holes, which tend to be more effective in the M_{bh}–M_{star} rather than the M_{bh}–σ plane.

(v) The residuals in the scaling relations of AGN show clear evidence for a strong intrinsic dependence of black hole mass on velocity dispersion but not on (bulge or total) stellar mass (Fig. 5), in line with what observed in the sample of local inactive black holes (Shankar et al. 2016). These results support the finding of Bernardi et al. (2005) and Bernardi et al. (2011), who showed that σ is the main driver of scaling relations with M_{star}.

REFERENCES

Alexander D. M., Hickox R. C., 2012, New Astron. Rev., 56, 93
Baldassare V. F. et al., 2016, ApJ, 829, 57
Baldi R. D. et al., 2018, MNRAS, 476, 3478
Barausse E., Shankar F., Bernardi M., Dubois Y., Sheth R. K., 2017, MNRAS, 468, 4782
Batcheldor D., 2010, ApJ, 711, L108
Batiste M., Bentz M. C., Raimundo S. I., Vestergaard M., Onken C. A., 2017, ApJ, 838, L10
Beifiori A., Courteau S., Corsini E. M., Zhu Y., 2012, MNRAS, 419, 2497
Bell E. F., de Jong R. S., 2001, ApJ, 550, 212
Bell E. F., McIntosh D. H., Katz N., Weinberg M. D., 2003a, ApJ, 585, L117
Bell E. F., McIntosh D. H., Katz N., Weinberg M. D., 2003b, ApJS, 149, 289
Bennert V. N., Auger M. W., Treu T., Woo J.-H., Malkan M. A., 2011, ApJ, 726, 59
Bentz M. C., Katz S., 2015, PASP, 127, 67
Bentz M. C., Manne-Nicholas E., 2018, ApJ, 864, 146
Bentz M. C., Peterson B. M., Pogge R. W., Vestergaard M., Onken C. A., 2006, ApJ, 644, 133
Bernardi M., Sheth R. K., Nichol R. C., Schneider D. P., Brinkmann J., 2005, AJ, 129, 61
Bernardi M., Sheth R. K., Tundo E., Hyde J. B., 2007, ApJ, 660, 267
Bernardi M., Shankar F., Hyde J. B., Mei S., Marulli F., Sheth R. K., 2010, MNRAS, 404, 2087
Bernardi M., Roche N., Shankar F., Sheth R. K., 2011, MNRAS, 412, L6
Bernardi M., Meert A., Sheth R. K., Vikram V., Huertas-Company M., Mei S., Shankar F., 2013, MNRAS, 436, 697
Bernardi M., Meert A., Vikram V., Huertas-Company M., Mei S., Shankar F., Sheth R. K., 2014, MNRAS, 443, 874
Bernardi M., Meert A., Sheth R. K., Fischer J.-L., Huertas-Company M., Maraston C., Shankar F., Vikram V., 2017, MNRAS, 467, 2217
Bernardi M., Meert A., Vikram V., Huertas-Company M., Mei S., Shankar F., Sheth R. K., 2017a, MNRAS
Bernardi M. et al., 2017b, MNRAS, 475, 757
Blandford R. D., McKee C. F., 1982, ApJ, 255, 419
Blanton M. R., Roweis S., 2007, AJ, 133, 734
Bonchi A., La Franca F., Melini G., Bongiorno A., Fiore F., 2013, MNRAS, 429, 1970
Bongiorno A. et al., 2014, MNRAS, 443, 2077
Bruzual G., Charlot S., 2003, MNRAS, 344, 1000
Busch G. et al., 2014, A&A, 561, A140
Cappellari M. et al., 2006, MNRAS, 366, 1126
Chabrier G., 2003, PASP, 115, 763
Chang Y.-Y. et al., 2017, ApJS, 233, 19
Chen S., Sesana A., Conselice C. J., 2018, preprint(arXiv:e-prints)
Chen Y.-C., Hwang C.-Y., 2017, Ap&SS, 362, 230
Collin S., Kawaguchi T., Peterson B. M., Vestergaard M., 2006, A&A, 456, 75
Consolandi G., 2016, A&A, 595, A67
Dasyra K. M. et al., 2007, ApJ, 657, 102
Delvecchio I. et al., 2017, A&A, 602, A3
Fabian A. C., 1999, MNRAS, 308, L39

Falomo R., Bettoni D., Karhunen K., Kotilainen J. K., Uslenghi M., 2014, MNRAS, 440, 476

Ferrarese L., Ford H., 2005, Space Sci. Rev., 116, 523

Ferrarese L., Pogge R. W., Peterson B. M., Merritt D., Wandel A., Joseph C. L., 2001, ApJ, 555, L79

Graham A. W., 2016, in Astrophysics and Space Science Library, Vol. 418, Galactic Bulges. Springer, Switzerland, p. 263

Graham A. W., Onken C. A., Athanassoula E., Combes F., 2011, MNRAS, 412, 2211

Graham A. W., Soria R., Davis B. L., 2019, MNRAS, 484, 814

Granato G. L., De Zotti G., Silva L., Bressan A., Danese L., 2004, ApJ, 600, 580

Greene J. E., Ho L. C., 2005, ApJ, 630, 122

Greene J. E. et al., 2016, ApJ, 826, L32

Grier C. J. et al., 2013, ApJ, 773, 90

Grier C. J., Pancoast A., Barth A. J., Fausnaugh M. M., Brewer B. J., Treu T., Peterson B. M., 2017, ApJ, 849, 146

Gültekin K. et al., 2009, ApJ, 698, 198

Ho L. C., Kim M., 2014, ApJ, 789, 17

Huertas-Company M., Aguerri J. A. L., Bernardi M., Mei S., Sánchez Almeida J., 2011, A&A, 525, A157

Into T., Portinari L., 2013, MNRAS, 430, 2715

Joshi B. C. et al., 2018, J. Astrophys. Astron., 39, 51

Kauffmann G., Heckman T. M., 2009, MNRAS, 397, 135

Kauffmann G., White S. D. M., Heckman T. M., Ménard B., Brinchmann J., Charlot S., Tremonti C., Brinkmann J., 2004, MNRAS, 353, 713

Kim M., Ho L. C., Peng C. Y., Barth A. J., Im M., Martini P., Nelson C. H., 2008, ApJ, 687, 767

King A., 2003, ApJ, 596, L27

Kormendy J., Ho L. C., 2013, ARA&A, 51, 511

Koss M. et al., 2017, ApJ, 850, 74

Kroupa P., 2001, MNRAS, 322, 231

Krumpe M., Miyaji T., Coil A. L., Aceves H., 2018, MNRAS, 474, 1773

La Franca F., Melini G., Fiore F., 2010, ApJ, 718, 368

Lamperti I. et al., 2017, MNRAS, 467, 540

Läsker R., Ferrarese L., van de Ven G., Shankar F., 2014, ApJ, 780, 70

Longhetti M., Saracco P., 2009, MNRAS, 394, 774

Martín-Navarro I., Mezcua M., 2018, ApJ, 855, L20

Mathur S., Fields D., Peterson B. M., Grupe D., 2012, ApJ, 754, 146

McConnell N. J., Ma C.-P., 2013, ApJ, 764, 184

Meert A., Vikram V., Bernardi M., 2015, MNRAS, 446, 3943

Meidt S. E. et al., 2014, ApJ, 788, 144

Mendel J. T., Simard L., Ellison S. L., Patton D. R., 2013, MNRAS, 429, 2212

Merloni A., Heinz S., di Matteo T., 2003, MNRAS, 345, 1057

Merritt D., Ferrarese L., 2001a, in Knapen J. H., Beckman J. E., Shlosman I., Mahoney T. J., eds, ASP Conf. Ser. Vol. 249, The Central Kiloparsec of Starbursts and AGN: The La Palma Connection. Astron. Soc. Pac., San Francisco, p. 335

Merritt D., Ferrarese L., 2001b, ApJ, 547, 140

Mezcua M., 2017, Int. J. Mod. Phys. D, 26, 1730021

Morabito L. K., Dai X., 2012, ApJ, 757, 172

Nelson C. H., Whittle M., 1995, ApJS, 99, 67

Nelson C. H., Green R. F., Bower G., Gebhardt K., Weistrop D., 2004, ApJ, 615, 652

Nucita A. A., Manni L., De Paolis F., Giordano M., Ingrosso G., 2017, ApJ, 837, 66

Onken C. A., Ferrarese L., Merritt D., Peterson B. M., Pogge R. W., Vestergaard M., Wandel A., 2004, ApJ, 615, 645

Pacucci F., Loeb A., Mezcua M., Martín-Navarro I., 2018, ApJ, 864, L6

Pancoast A., Brewer B. J., Treu T., 2014, MNRAS, 445, 3055

Paturel G., Petit C., Prugniel P., Theureau G., Rousseau J., Brouty M., Dubois P., Cambrésy L., 2003, A&A, 412, 45

Penny S. J. et al., 2018, MNRAS, 476, 979

Peterson B. M., 1993, PASP, 105, 247

Peterson B. M. et al., 2004, ApJ, 613, 682

Reines A. E., Volonteri M., 2015, ApJ, 813, 82

Ricci F. et al., 2017a, MNRAS, 471, L41

Ricci F., La Franca F., Onori F., Bianchi S., 2017b, A&A, 598, A51

Rowan-Robinson M. et al., 2017, A&A, 619, A169

Saglia R. P. et al., 2016, ApJ, 818, 47

Sarria J. E., Maiolino R., La Franca F., Pozzi F., Fiore F., Marconi A., Vignali C., Comastri A., 2010, A&A, 522, L3

Savorgnan G. A. D., Graham A. W., 2016, ApJS, 222, 10

Schulze A., Wisotzki L., Husemann B., 2009, A&A, 507, 781

Sérsic J. L., 1963, Bol. Asociacion Argentina Astron. Plata Argentina, 6, 41

Sesana A., Shankar F., Bernardi M., Sheth R. K., 2016, MNRAS, 463, L6

Shankar F., 2009, New Astron. Rev., 53, 57

Shankar F., Weinberg D. H., Miralda-Escudé J., 2013, MNRAS, 428, 421

Shankar F. et al., 2016, MNRAS, 460, 3119

Shankar F., Bernardi M., Sheth R. K., 2017, MNRAS, 466, 4029

Sheth R. K., Bernardi M., 2012, MNRAS, 422, 1825

Silk J., Rees M. J., 1998, A&A, 331, L1

Taylor S. R., Simon J., Sampson L., 2017, Phys. Rev. Lett., 118, 181102

van den Bosch R. C. E., 2016, ApJ, 831, 134

van den Bosch R. C. E., Gebhardt K., Gültekin K., Yıldırım A., Walsh J. L., 2015, ApJS, 218, 10

Walsh J. L. et al., 2009, ApJS, 185, 156

, Williams P. R. et al., 2018, ApJ, 866, 75, ()

Woo J.-H. et al., 2010a, ApJ, 716, 269

Woo J.-H. et al., 2010b, ApJ, 716, 269

Woo J.-H., Schulze A., Park D., Kang W.-R., Kim S. C., Riechers D. A., 2013a, ApJ, 772, 49

Woo J.-H., Schulze A., Park D., Kang W.-R., Kim S. C., Riechers D. A., 2013b, ApJ, 772, 49

Woo J.-H., Yoon Y., Park S., Park D., Kim S. C., 2015, ApJ, 801, 38

York D. G. et al., 2000, AJ, 120, 1579(SDSS)

Zibetti S., Charlot S., Rix H.-W., 2009, MNRAS, 400, 1181

APPENDIX A: AGN SAMPLES USED IN THE MAIN TEXT

We here describe how we have corrected the stellar and black hole masses to a *homogeneous* system in our reference AGN samples. As in the main text, we here always refer to f_{vir} as the virial factor calibrated on the line dispersion (i.e. second moment of the line profile) of Hβ (e.g. Peterson et al. 2004). For virial black hole masses calibrated adopting the FWHM of the Hα line, we will instead denote the virial factors with the symbol ϵ, following the convention put forward by Onken et al. (2004), which is roughly a factor of a few lower than f_{vir}. All the AGN samples considered in this work adopt as a reference the line dispersion of the broad Hβ emission line, except for the samples by Reines & Volonteri (2015) and Martín-Navarro & Mezcua (2018), who adopt the FWHMs of the Hα lines. Grier et al. (2017) have fitted the continuum Hβ emission-line spectra finding that $f_{vir} \sim 3.5 \,(\log f_{vir} = 0.54 \pm 0.17)$ and $\epsilon \sim 1.5 \,(\log \epsilon = 0.18 \pm 0.23)$ when adopting the line dispersion and FWHM of the Hβ line, respectively. Following Grier et al. (2017), in this work we use as our (mean) reference virial factors $f_{vir} = 3.5$ and $\epsilon = 1.51$. When adopting larger values of f_{vir} (e.g. as in the right-hand panels of Fig. 2), we increase our reference ϵ proportionally to the ratio $f_{vir}/3.5$. We here assume the same equivalent virial factors apply to both the Hα and the Hβ emission lines. This is corroborated by Greene & Ho (2005), who found a tight linear correlation between the Hα and Hβ FWHMs with only a relatively small offset of $\lesssim 0.05$ dex between the two lines (their fig. 3), and also more recently by Ricci et al. (2017b, their fig. 1). This offset would correspond to a systematic difference in the implied black hole masses of $\lesssim 25$ per cent, which is much lower than the level of systematics discussed in this work. We now provide a brief description of each of the AGN samples considered in this work:

(1) Reines & Volonteri ([2015]) carried out a study of the black hole mass–host galaxy stellar mass relation of 262 broad-line AGN at $z \leq 0.055$, from the SDSS. Stellar masses were derived from the Zibetti, Charlot & Rix ([2009]) colour-dependent mass-to-light ratios. After correcting for a different IMF, Reines & Volonteri ([2015]) showed that the Zibetti et al. ([2009]) stellar masses present a mass-dependent offset with respect to the Bell et al. ([2003b]) stellar masses (their fig. 6, upper panel) that we approximate as

$$\log M_{\text{star,Bell}} = 1.793 + 0.845 \times \log M_{\text{star,Zib}}, \qquad \text{(A1)}$$

which provides, in the range of interest here $9 < \log M_{\text{star}} < 11.5$, a median offset of ~ 0.21 dex, as measured by Reines & Volonteri ([2015]). Reines & Volonteri ([2015]) calculated black hole masses from single-epoch virial estimators based on the Hα emission line and luminosity, with a mean virial coefficient $\epsilon = 1.075$ (Onken et al. [2004]; Grier et al. [2013]), which we correct to our reference value of $\epsilon = 1.51$.

(2) Ho & Kim ([2014]) collected 43 reverberation mapping AGN with Sérsic (Sérsic [1963]) bulge-to-total decompositions on *Hubble Space Telescope* imaging. Bulge masses were then computed from the $B - R$ colour-dependent M_{star}/L from Bell et al. ([2003b]), and converted to total stellar masses using their tabulated values of bulge-to-total fractions. Bell et al. ([2003b]) adopted a 'diet Salpeter' IMF, which we corrected to our reference Chabrier IMF subtracting 0.1 dex to all stellar masses (see table 2 in Bernardi et al. [2010]). We assign to all their stellar masses a typical statistical error of 0.15 dex (Bernardi et al. [2014]). Ho & Kim ([2014]) took bulge velocity dispersions mostly from Nelson et al. ([2004]) and Woo et al. ([2013b]), who calibrated their velocity dispersions specifically at the effective radius. Other measurements adopted by Ho & Kim ([2014]) are from, e.g. Nelson & Whittle ([1995]), Ferrarese et al. ([2001]), or Woo et al. ([2010b]), who extracted spectra from 2 arcsec slits or a few arcsecond square apertures centred on the nucleus, similar to the aperture adopted in SDSS galaxies. As discussed by Ferrarese et al. ([2001]) and Nelson et al. ([2004]), these velocity dispersion measurements are effectively carried out at several kiloparsecs from the centre, probe the stellar bulge potential, and show relatively flat profiles (e.g. Merritt & Ferrarese [2001b]; Kormendy & Ho [2013]). We thus treat all their measured velocity dispersions as equivalent to those in our SDSS sample within one effective radius. As a further test, we also checked that fully consistent results are found in both the σ–M_{star} relation (Fig. [1]) and residuals (Fig. [5]), when adopting, wherever possible, velocity dispersions from the Hyperleda data base (Paturel et al. [2003]). Ho & Kim ([2014]) divided their sample into classical and pseudobulges based on their Sérsic index, for which they calibrated, respectively, $f_{\text{vir}} = 6.3$ and $f_{\text{vir}} = 3.2$ (based on the Hβ line dispersion) when compared to the local M_{bh}–σ relation of inactive galaxies from Kormendy & Ho ([2013]). We instead adopt for all black hole masses in their sample a constant $f_{\text{vir}} = 3.5$.

(3) Busch et al. ([2014]) performed aperture photometry and bulge-to-disc decompositions on near-infrared *J*-, *H*-, and *K*-band images of 20 low-luminosity type-1 quasars at $z \leq 0.06$ from the Hamburg/ESO survey. Stellar masses were calculated from parametric models based on inactive galaxy colours and using the Bell et al. ([2003b]) mass-to-light ratios, which we again correct to our reference Chabrier IMF subtracting 0.1 dex. Black hole masses were derived from the Hβ line dispersion virial-based sample of Schulze, Wisotzki & Husemann ([2009]) with $f_{\text{vir}} = 3.85$ (Collin et al. [2006]), which we rescale to $f_{\text{vir}} = 3.5$.

(4) Greene et al. ([2016]) presented black hole masses and stellar velocity dispersion measurements for several local megamaser

early-to-mid-type spiral galaxies, including those from the Saglia et al. ([2016]) sample. Black hole masses were derived by fitting a Keplerian rotation curve to the positions and velocities of the maser spots. Using SDSS data, stellar masses were obtained from the Bell et al. ([2003b]) mass-to-light ratios, for which we subtract a constant 0.1 dex. Velocity dispersions were extracted from spectra within a 2 arcsec aperture and were measured from the first two moments of the line-of-sight velocity dispersion. Analogously to the Ferrarese et al. ([2001]) measurements, even for this sample we do not apply any correction to the velocity dispersions when comparing to the SDSS σ_e.

(5) Martín-Navarro & Mezcua ([2018]) studied 127 low-mass Seyfert 1 galaxies with measured stellar masses from the SDSS spectral measurements and Bruzual & Charlot ([2003]) libraries with a Chabrier IMF, which are fully consistent with the stellar masses from Kauffmann et al. ([2004]) and systematically lower than those calibrated using Bell et al. ([2003b]) by ~ 0.25 dex (e.g. Bernardi et al. [2016]). Black hole masses, derived from the Hα virial relations of Woo et al. ([2015], and references therein) with a mean virial factor of $\epsilon = 1.12$ and $\epsilon = 0.75$, respectively, are converted to our reference $\epsilon = 1.51$. Velocity dispersions were extracted from SDSS and corrected for an aperture within one (exponential) effective radius via the usual scaling

$$\sigma(R_e) = \sigma_{\text{SDSS}}(1.5 \text{ arcsec}) \times \left(\frac{1.5 \text{ arcsec}}{R_e} \right)^{\gamma}, \qquad \text{(A2)}$$

but using a Sérsic index-dependent slope (Bernardi et al. [2017b])

$$\gamma = -0.016366723 + 0.019136886 \times n_{\text{Ser}} \qquad \text{(A3)}$$
$$-0.0010648890 \times (n_{\text{Ser}})^2 .$$

We set the Sérsic index $n_{\text{Ser}} = 1$ in equation (A3), as the vast majority of the Martín-Navarro & Mezcua ([2018]) sample is heavily disc dominated. Assuming a larger value for the Sérsic index such as $n_{\text{Ser}} = 2$ has a negligible effect on our results.

(6) van den Bosch ([2016]) compiled one of the largest samples of active and inactive supermassive black holes from the literature, counting 230 sources with black hole mass measurements from stellar dynamics, gas or CO dynamics, masers, and reverberation mapping-based relations. In what follows, we will only consider the active galaxies from van den Bosch ([2016]) from masers and reverberation-based estimates. The latter are extracted from the original sample by Bentz & Katz ([2015]) who adopted a mean $f_{\text{vir}} = 4.31$ from Grier et al. ([2013]; Hβ line dispersion), which we rescale to $f_{\text{vir}} = 3.5$. van den Bosch ([2016]) adopted, wherever possible, the closest approximation to σ_e for the velocity dispersions (to which we assign typical statistical errors of 0.05 dex, Bernardi et al. [2010]), and uniformly applied Sérsic fits to the 2MASS K_s-band photometry. All galaxies in this sample, which excludes the most massive galaxies, are well resolved and detected in 2MASS according to van den Bosch ([2016]). Following van den Bosch ([2016]), galaxy luminosities were then converted to stellar masses via the velocity dispersion-dependent mass-to-light ratio from Kormendy & Ho ([2013]):

$$\frac{M_{\text{star}}}{L_K} = K_0 \left(\frac{\sigma_e}{166 \text{ km s}^{-1}} \right)^{0.45} \frac{M_\odot}{L_{\odot,\text{K}}} . \qquad \text{(A4)}$$

Kormendy & Ho ([2013]) specify that the constant in equation (A4) should be $K_0 \sim 1$ for the total *dynamical* mass-to-light ratios, and further detail that, following Into & Portinari ([2013]), it should be reduced to $K_0 \sim 0.76$ when considering, as in this work, only the stellar component. We thus adopt the latter value for K_0. We further subtract a constant 0.05 dex from all stellar masses to account

for the heavier (Kroupa 2001) IMF adopted by Into & Portinari (2013). In the end, we find that galaxies with a Chabrier IMF and $\sigma_e = 166\,\mathrm{km\,s^{-1}}$ have an average $M_{\mathrm{star}}/L_K \sim 0.676$, which is in excellent agreement with the mean $M_{\mathrm{star}}/L_K = 0.67$ calculated by Longhetti & Saracco (2009). Indeed, we checked that equivalent results are found throughout even ignoring the (weak) dependence on velocity dispersion in equation (A4). We note that the van den Bosch (2016) maser subsample also includes the sources from Greene et al. (2016) but with independent measurements of the host stellar masses so we will still consider them as fully independent estimates.

(7) Bentz & Manne-Nicholas (2018) recently collected a sample of 37 active galaxies with high-resolution optical images from the *Hubble Space Telescope* with reverberation-based black hole masses with an average $f_{\mathrm{vir}} = 4.3$. Total luminosities are derived from Sérsic fits, though with a Sérsic index capped at $n_{\mathrm{Ser}} \leq 4$. We consider their mass-to-light ratios from Bell & de Jong (2001), who adopted a diet Salpeter. However, in this specific instance we do not subtract their stellar masses by 0.1 dex to convert to a Chabrier IMF as Bell et al. (2003b) showed (their fig. 20, left-hand panel) that at fixed optical galaxy colour the Bell & de Jong (2001) M_{star}/L are already systematically underestimated by (at least) $\sim$0.1 dex with respect to those from Bell et al. (2003b).

Other AGN samples are available in the local Universe but are less suited to our purposes. For example, Nucita et al. (2017) presented X-ray AGN at $z \leq 0.055$ with black hole masses derived from the X-ray/radio Fundamental Plane relation (Merloni, Heinz & di Matteo 2003). However, the latter has already been shown to be biased, probably tracing the upper envelope of a much broader distribution (e.g. La Franca, Melini & Fiore 2010; Bonchi et al. 2013; Baldi et al. 2018; Martín-Navarro & Mezcua 2018). Koss et al. (2017) presented the first catalogue and data release of the Swift BAT AGN Spectroscopic Survey. However, their stellar masses were obtained by combining the SDSS Petrosian photometry with the Blanton & Roweis (2007) mass-to-light ratios both of which contribute to yield stellar masses a factor of $\gtrsim 2$ lower than the updated measurements adopted here (e.g. Bernardi et al. 2010, 2013). Nevertheless, we checked that after correcting stellar masses by a factor of 2 the Koss et al. (2017) sample lies well below the observed $M_{\mathrm{bh}}-M_{\mathrm{star}}$ relation of quiescent galaxies. Interestingly, Lamperti et al. (2017, see also fig. 8 in Krumpe et al. 2018) point to a discrepancy of up to an order of magnitude between black hole masses measured from virial relations and the $M_{\mathrm{bh}}-\sigma$ relation, in full agreement with the main conclusion of this work.

This paper has been typeset from a T_EX/L^AT_EX file prepared by the author.